

LIGHT PROPAGATION: FROM ATOMIC TO NUCLEAR QUANTUM OPTICS

J. EVERS*, R. FLEISCHHAKER, A. PÁLFFY and C. H. KEITEL

*Max Planck Institute for Nuclear Physics
Saupfercheckweg 1, 69117 Heidelberg, Germany*

** E-mail: joerg.evers@mpi-hd.mpg.de
<http://www.mpi-hd.mpg.de/~evers/>*

Coherent control of light propagation in atomic and nuclear media is discussed. The main focus is on light propagation through so-called closed-loop media. We present a calculation technique which allows to evaluate and interpret the light propagation dynamics in closed-loop media. As an application, we discuss the realization of a so-called white-light cavity with artificially enhanced bandwidth. We further study light propagation in media which realize a cross-coupling of the electric and the magnetic probe field component. Finally, we discuss coherent control of nuclear forward scattering, as an example for light propagation in nuclear media.

Keywords: Quantum optics, light propagation, closed-loop media, chiral media, nuclear quantum optics.

1. Introduction

Light propagation through coherently prepared media is a cornerstone of research and applications in quantum optics. In particular, electromagnetically induced transparency (EIT) allows for the propagation with low absorption, controlled velocity and the storage of light pulses, together with other beneficial properties such as high nonlinear response.¹ Consequently, based on the idea of EIT, a great variety of model systems have been analyzed. Here, we will mainly discuss a particular class of level schemes, which are so-called loop systems.²⁻⁷ In these media, the applied laser fields form a closed interaction loop. As a consequence, in such systems a certain initial atomic state is connected to a final atomic state via several different combinations of laser field interactions. On the one hand, this leads to quantum pathway interference, and thus to a dependence of the system properties on the relative phase of the driving fields. This allows for a efficient control

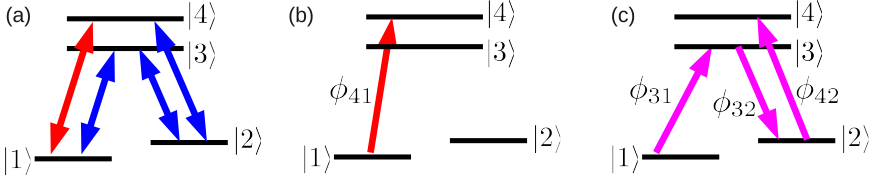


Fig. 1. (a) The four-level double- Λ type scheme with laser fields applied in closed-loop configuration. (b) and (c) are two possible interfering pathways from $|1\rangle$ to $|4\rangle$.

of the optical properties. On the other hand, however, such a system in general does not have a time-independent steady state.

In the following, first, we present a theory to describe light propagation in closed loop media. As an application, we discuss a so-called white light cavity. Next, we address light propagation in media that cross-couple the electric and the magnetic component of a single probe field, which can be seen as an ideal implementation of a closed-loop medium. Finally, we describe possible extensions of light propagation to nuclear systems.

2. Closed-Loop Media

An example for a closed-loop level scheme is given in Fig. 1. Starting from state $|1\rangle$, it is possible to evolve the atomic population by laser fields via states $|3\rangle$, $|2\rangle$ and $|4\rangle$ back to the initial state $|1\rangle$, such that the condition for a closed-loop system is fulfilled. Interference thus can occur, for example, between the pathways $|1\rangle \rightarrow |4\rangle$ and $|1\rangle \rightarrow |3\rangle \rightarrow |2\rangle \rightarrow |4\rangle$. Mathematically, the closed-loop property implies that it is impossible to find an interaction picture in which the Hamiltonian does not have an explicit time dependence. In a suitable interaction picture, the Hamiltonian can be written in the simple form V given by

$$V = \hbar(\Delta_{32} - \Delta_{31})\tilde{\rho}_{22} - \hbar\Delta_{31}\tilde{\rho}_{33} + \hbar(\Delta_{32} - \Delta_{31} - \Delta_{42})\tilde{\rho}_{44} - \hbar(g_{31}\tilde{\rho}_{31} + g_{32}\tilde{\rho}_{32} + g_{42}\tilde{\rho}_{42} + g_{41}\tilde{\rho}_{41}e^{-i\Phi} + \text{h.c.}). \quad (1)$$

Here, $\tilde{\rho}_{ij}$ is the operator $|i\rangle\langle j|$ in the chosen reference frame ($i, j \in \{1, \dots, 4\}$). The Rabi frequencies are g_{ij} , and Δ_{ij} are laser field detunings. In this interaction picture, the residual time dependence along with the laser field phases appears only together with the Rabi frequency g_{41} , which we associate to a weak probe field coupled to transition $|1\rangle \leftrightarrow |4\rangle$.

The parameter Φ is given by

$$\Phi = \Delta t - \vec{K}\vec{r} + \phi_0, \quad \Delta = (\Delta_{32} + \Delta_{41}) - (\Delta_{31} + \Delta_{42}), \quad (2a)$$

$$\vec{K} = (\vec{k}_{32} + \vec{k}_{41}) - (\vec{k}_{31} + \vec{k}_{42}), \quad \phi_0 = (\phi_{32} + \phi_{41}) - (\phi_{31} + \phi_{42}). \quad (2b)$$

The parameters Δ , \vec{K} and ϕ_0 are known as the multiphoton resonance detuning, wave vector mismatch and initial phase difference, respectively. These parameters are a direct consequence of the closed-loop nature. In general it is not possible to find a reference frame where the explicit time dependence due to Δ vanishes from the Hamiltonian, such that for $\Delta \neq 0$ no stationary long-time limit can be expected. Therefore, a time-dependent solution of the density matrix equations is required. Using the notation $\bar{g}_{41} = g_{41} \exp[-i\vec{K}\vec{r} + i\phi_0]$, the density matrix equations of motion can be written as

$$\frac{\partial}{\partial t} \tilde{R} + \Sigma = M \tilde{R}, \quad (3)$$

where \tilde{R} is a vector containing the density matrix elements. M is a time-dependent matrix, and Σ a time-dependent vector independent of the density matrix elements which arises from eliminating one of the state populations from the equations of motion via the trace condition $Tr(\tilde{\rho}) = 1$. For a weak probe field, using Floquet's theorem,⁸ the solution \tilde{R} can be obtained with a series ansatz

$$\tilde{R} = \tilde{R}_0 + \bar{g}_{41} e^{-i\Delta t} \tilde{R}_1 + \bar{g}_{41}^* e^{i\Delta t} \tilde{R}_{-1} + \dots, \quad (4)$$

where \tilde{R}_i ($i \in \{0, \pm 1, \dots\}$) are time-independent coefficient vectors. Using this ansatz, the time-dependent solution to the density matrix equations of motion can be found, which allows to evaluate all observables.^{6,9}

In an interaction picture oscillating in phase with the applied probe field, the probe field transition coherence $\hat{\rho}_{41}$ determining the light pulse propagation through the medium can be written as,

$$\hat{\rho}_{41} = [\tilde{R}_0]_p e^{i\Phi} + g_{41} [\tilde{R}_1]_p + g_{41}^* [\tilde{R}_{-1}]_p e^{2i\Phi}, \quad (5)$$

where $[x]_{13}$ denotes the relevant probe field coherence component of the vector x .⁶ The different contributions to this result naturally arising from the Floquet analysis correspond to the various involved physical processes and allow to in detail understand the medium response. The first part of Eq. (5) represents the scattering of the driving fields into the probe field mode arises from $[\tilde{R}_0]_p$, as shown in Fig. 2(a). This contribution in general does not oscillate at the probe field frequency, but rather at the combination frequency $\omega_{31} + \omega_{42} - \omega_{32}$ of the three driving fields. This

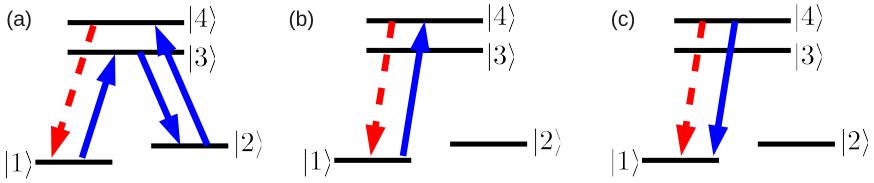


Fig. 2. (Color online) Interpretation of the different contributions to the probe field susceptibility in terms of transition pathways. (a) represents the interaction loop leading to a scattering of the driving fields into the probe field mode. (b) is the direct scattering of the probe field off of the probe transition. (c) shows a counter-rotating term. The solid blue arrows indicate coupling field transitions, the dashed red line is a probe field interaction.

frequency coincides with the probe field frequency only under multiphoton resonance. The contribution proportional to $[\tilde{R}_1]_p$ shown in Fig. 2(b) is in phase with the probe field for all values of Δ , and is independent of the relative field phase. It represents the direct scattering of the probe field off of the probe field transition. The third contribution proportional to $[\tilde{R}_{-1}]_p$ can be interpreted as a counter-rotating term which in the Floquet expansion differs by 2Δ from the probe field frequency, and is depicted in Fig. 2(c).

As an important result, it can be concluded that the phase-dependence of the loop-configuration studied here is restricted to the multiphoton resonance condition $\Delta = 0$, because it arises from the scattering of the coupling fields into the probe field mode. Furthermore, it can be seen from Eq. (5) that all contributions but the direct scattering acquire an additional dependence on the wave vector mismatch \vec{K} together with the dependence on the phase ϕ_0 . Therefore, the laser field geometry influences the relevance of these contributions to the detection signal in probe field propagation direction. In general, only the direct scattering contribution can be detected in propagation direction of the probe beam regardless of the separation of detector and the scattering atoms.

The considered system enables one to control the pulse propagation to a great extent.⁶ An example is shown in Fig. 3. In (a), around zero probe field detuning, subluminal light propagation with gain could be realized. At $\Delta_{41} \approx \pm 2\gamma_0$, superluminal propagation with small absorption or gain occurs. (b) shows an example of switching between sub- and superluminal light propagation by via the value of one of the coupling field Rabi frequencies. The interesting range around is accompanied by vanishing absorption at $\Delta_{41} = 0$.

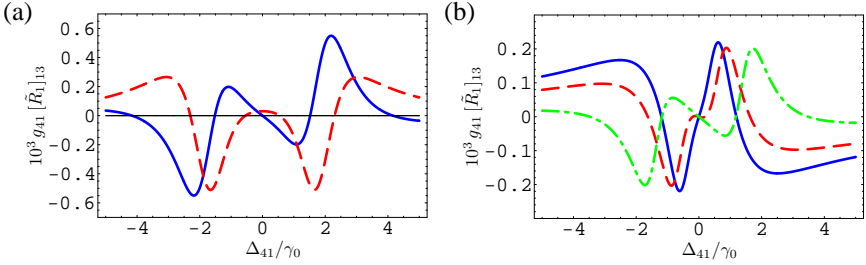


Fig. 3. Results for the susceptibility in the closed-loop system. Both curves show the direct scattering channel indicated in Fig. 2(b). (a) the parameters are $g_{31} = 1.8\gamma_0$, $g_{32} = 0.2\gamma_0$, $g_{42} = 0.5\gamma_0$, and $g_{41} = 0.01\gamma_0$. (b) shows results for different Rabi frequencies of the coupling field g_{31} , namely, $g_{31} = 0.7\gamma_0$ (solid line), $g_{31} = 0.85\gamma_0$ (dashed line), and $g_{31} = 1.5\gamma_0$ (dash-dotted line). The other couplings are $g_{42} = 0.2\gamma_0$, and $g_{41} = 0.01\gamma_0$. In both subfigures, the detunings and decay rates are $\Delta_{31} = \Delta_{32} = \Delta_{42} = 0$, and $2\gamma_{13} = 2\gamma_{14} = 2\gamma_{23} = 2\gamma_{24} = \gamma_0$.

3. An “Open” Closed Loop System

Interesting insight in the dynamics of light propagation can be gained by considering the closed-loop setup shown in Fig. 1 without the driving field coupling to transition $|2\rangle \leftrightarrow |3\rangle$.⁹ Then, the driving fields no longer form a closed loop. Also, naively, one would expect strong absorption to occur, for example, since the EIT formed on resonance in the Λ -type subsystem $|1\rangle$, $|4\rangle$ and $|2\rangle$ is constantly perturbed by the driving field between $|1\rangle$ and $|3\rangle$. The absorption of the control fields is symbolically depicted in Fig. 4(a). A more thorough analysis shows that two additional processes need to be considered, as shown in Fig. 4(b,c). Due to a four-wave mixing (4WM) process, an additional field is generated on the undriven transition $|2\rangle \leftrightarrow |3\rangle$ throughout the propagation, as shown in (b). This dynamically generated field then leads to a second 4WM process that scatters the newly created field and the control fields back into the probe field mode. A full numerical solution of the corresponding Maxwell-Schrödinger propagation equations for a probe field pulse reveals that the interplay of these processes in effect leads to a slight gain of the probe field throughout the propagation. The control fields, on the other hand, are substantially absorbed throughout the propagation, while at the same time the amplitude of the 4WM field builds up. Despite this pronounced in-medium dynamics, the effective susceptibility experienced by the probe pulse over the whole propagation can be surprisingly smooth.⁹

As an application, such a medium allows to construct a so-called white-light cavity (WLC).^{9–12} A regular optical cavity has a finite bandwidth of

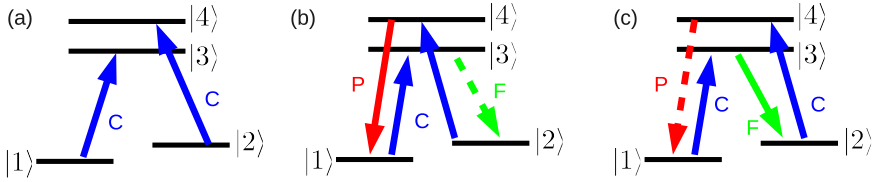


Fig. 4. Main contributions to the in-medium propagation dynamics. (a) absorption of the coupling fields (C). (b) four-wave mixing of coupling fields and probe field (P) to give an additional field (F). (c) “backscattering” of coupling and four-wave-mixing field into the probe field mode.

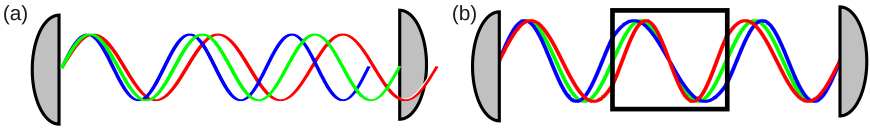


Fig. 5. White light cavity mechanism. In (a), two of the three wavelengths are not supported by the cavity. In (b), the additional dispersive medium placed inside the cavity causes all three wavelengths to be supported by introducing suitable frequency-dependent phase shifts.

supported frequencies, as indicated in Fig. 5(a). Two of the shown waves do not fit into the resonator, and thus would not be supported by the cavity. However, if an additional medium with a suitable (negative) dispersion is introduced into the cavity, then the effective wavelength of the different frequency components may change. In particular, in subfigure (b), it can be seen that a suitable dispersion can transform all three different wavelengths into the supported frequency spectrum. This way, the bandwidth of a cavity can be enhanced, without reducing the maximum intensity buildup. More specific, in one round trip through a cavity of length L , a field with detuning Δ relative to the cavity resonance frequency will acquire a phase $\phi_0 = 2L\Delta/c$. If in addition a medium of length l and index of refraction n is introduced to the cavity, it will lead to an additional phase shift $\phi_1 = 2l\omega_0(n - 1)/c$, with ω_0 the resonance frequency. A white light cavity is achieved, if these phase shifts cancel, $\phi_0 + \phi_1 = 0$. This leads to a white-light cavity condition

$$\omega_0 \frac{\partial n(\omega_0)}{\partial \omega} = -\frac{L}{l}, \quad (6)$$

i.e., negative dispersion is required. Based on a full analysis of the above described system, it turns out that for a cavity length of about 59.5 cm, a medium length of 30 cm, and an empty cavity finesse of 1000, a medium

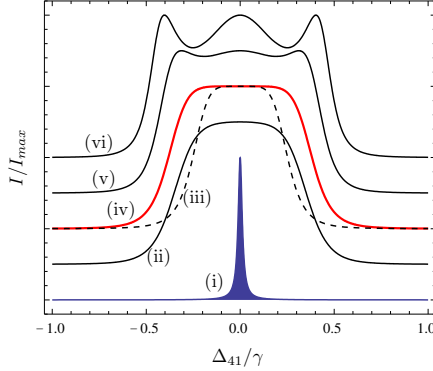


Fig. 6. Intensity profile of the white light cavity. The different cases are discussed in the text. Note that the curves all have the same base line, but are shifted in y direction in the figure for better visibility.

of the type described above driven by suitable coupling fields would allow to enhance the empty cavity bandwidth by a factor of about 30. In Fig. 6, curve (i) shows the empty cavity, and (iv) the corresponding curve with WLC medium. If the WLC-condition Eq. (6) is fulfilled, the cavity has a near-flat intensity distribution across the enhanced resonance width.⁹ Interestingly, the pronounced in-medium dynamics leads to an enhancement of the WLC cavity width, as can be seen from curve (iii), which is the result of a calculation with the 4WM processes artificially suppressed. In curves (ii), the WLC condition is overcompensated by 2%, while (vi) and (v) correspond to 2% and 4% overcompensation.

4. Light Propagation in Media with Cross Coupling of Electric and Magnetic Field Component

Motivated not least by ideas related to the realization of materials with a negative index of refraction in atomic gases, in the recent past, atomic level schemes have been considered which lead to a cross-coupling of the electric component \mathbf{E} and the magnetic component \mathbf{H} of a single probe laser field. In this case, the medium polarization $\mathbf{P}(t)$ and magnetization $\mathbf{M}(t)$ can be written as,

$$\mathbf{P}(t) = \int \left(\varepsilon_0 \chi_E(\tau) \mathbf{E}(t - \tau) + \frac{1}{c} \xi_{EH}(\tau) \mathbf{H}(t - \tau) \right) d\tau, \quad (7)$$

$$\mathbf{M}(t) = \int \left(\chi_H(\tau) \mathbf{H}(t - \tau) + \frac{1}{c\mu_0} \xi_{HE}(\tau) \mathbf{E}(t - \tau) \right) d\tau. \quad (8)$$

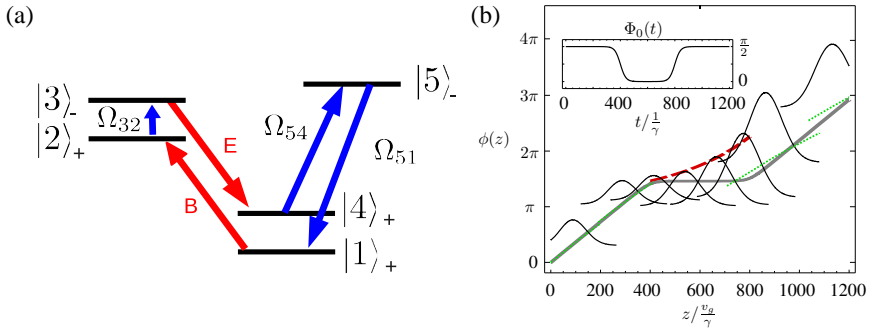


Fig. 7. (a) Level scheme featuring cross coupling of the electric and the magnetic field components of a probe beam. (b) Light propagation in the medium shown in (a). The figure shows the phase $\phi(z)$ of the central pulse component versus propagation distance z . The inset shows the applied closed-loop phase versus propagation time.

Here, χ_E and χ_M are the usual linear response coefficients for electric and magnetic field, respectively, while χ_{HE} and χ_{EH} describe the cross-coupling. It is interesting to note that a setup of this type essentially requires a closed-loop level scheme. A particular example is shown in Fig. 7(a).^{7,13} The two probe field components couple to transitions $|1\rangle \leftrightarrow |2\rangle$ and $|3\rangle \leftrightarrow |4\rangle$. Calculating the closed-loop phase for this setup, one obtains

$$\begin{aligned} \phi &= \phi_{\text{probe}} + \phi_{32} - \phi_{\text{probe}} + \phi_{54} - \phi_{51} \\ &= \phi_{32} + \phi_{54} - \phi_{51}. \end{aligned} \quad (9)$$

In contrast to regular closed-loop media which couple only to the electric component of the probe field, the closed-loop phase is independent of the applied probe field phase. The reason for this is that in one loop, one absorption and one emission of a probe field photon occur. This is a crucial advantage for potential applications, since then the properties of the probe pulse may not be known. In this sense, media with cross-coupling of electric and magnetic field component are ideal closed-loop media. Fig. 7(b) shows the result of a numerical solution to the full Maxwell-Schrödinger equations describing the pulse propagation through the medium shown in Fig. 7(a). The figure mainly depicts the phase in the center of the propagated pulse versus propagation length z . At the initial stage of the propagation, the phase increases linearly with z , which is due to a real index of refraction. At a certain time throughout the propagation, the closed-loop phase is changed, as shown in the inset. The pulse now propagates with constant phase, but with exponentially increasing pulse amplitude, which corresponds to an imaginary index of refraction with suitable sign. Finally,

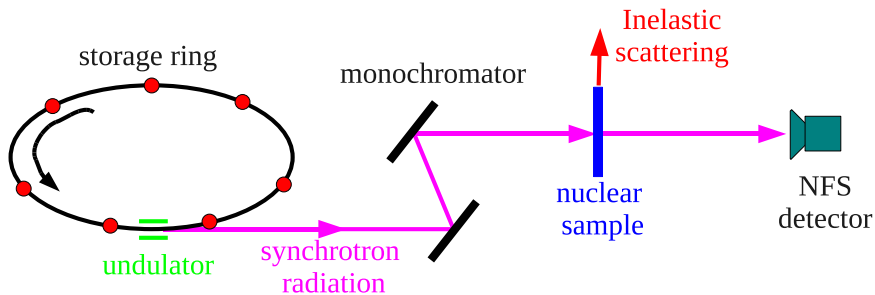


Fig. 8. Typical setup in nuclear forward scattering.

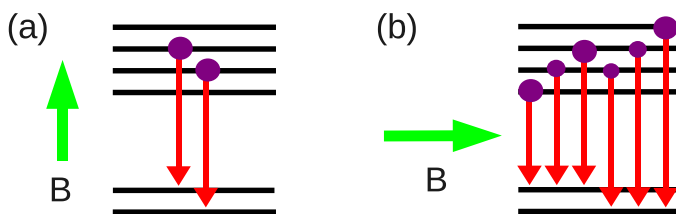


Fig. 9. Level scheme of ^{57}Fe after excitation with linearly polarized light. (a) with magnetic field as during the excitation. (b) with rotated magnetic field. The circles indicate population in the upper states.

at a later time, the closed-loop phase is switched back, and the pulse again propagates with constant amplitude, but with increasing phase. This result demonstrates that it is possible to dynamically influence the propagation dynamics of a probe pulse in a closed loop medium via the control field phases. At the same time, it is interesting to note that the additional coupling of the magnetic field component is crucial to the phase control, even though it is very weak. The reason is that only the magnetic field component allows to close the interaction loop, which becomes significant due to the strong coupling fields contributing to the other transitions in the loop, already at parameters compatible with state-of-the-art light propagation experiments.

5. Light Propagation in Nuclear Media

Coherent control of nuclear dynamics has been a long-term goal over the last few decades, fueled by the desire for a number of fascinating applications such as gamma-ray lasers or clean energy storage. However, not least

due to the lack of suitable light sources, a direct transfer of quantum optical schemes to the nuclear case is often not promising. We therefore here pursue a different approach, and study coherent control in a typical experimental setting for light scattering off of nuclei. In coherent nuclear forward scattering, intense high-frequency light such as that from a synchrotron radiation source is monochromatized at a nuclear resonance energy, and then hits a nuclear target, as shown schematically in Fig. 8.¹⁴ A detector placed in forward direction then registers the coherently scattered photons. The most commonly used target consists of ^{57}Fe , which has a magnetic dipole allowed Mößbauer transition from a $J = 1/2$ ground state to a $J = 3/2$ first excited state at 14.4 keV energy. At typical synchrotron source parameters, per incident light pulse at most one nucleus in the sample is excited. This low excitation rate is mostly due to the fact that the nuclear resonances are very narrow (~ 5 neV) compared to the bandwidth of the light after the monochromator (\sim meV). The coherently scattered light can be described with a wave equation similar to the atomic case,¹⁵

$$\left(\Delta - \frac{1}{c^2} \frac{\partial^2}{\partial t^2}\right) \vec{E} = \frac{4\pi}{c} \frac{\partial}{\partial t} \vec{I}, \quad (10)$$

where \vec{E} is the electric field of the light, and \vec{I} is the nuclear source current. In slowly varying envelope approximation, and for light propagating in z direction, this simplifies to an equation for the envelopes \mathcal{E} and \mathcal{I} given by

$$\frac{\partial}{\partial z} \vec{\mathcal{E}} = -\frac{2\pi}{c} \vec{\mathcal{I}}. \quad (11)$$

Calculating the nuclear source current in second order in the interaction of the light and the nuclei, one finally obtains a wave equation

$$\frac{\partial \vec{\mathcal{E}}(z, t)}{\partial z} = -\sum_{\ell} K_{\ell} \vec{J}_{\ell}(t) \int_{-\infty}^t d\tau \vec{J}_{\ell}^{\dagger}(\tau) \cdot \vec{\mathcal{E}}(z, \tau) \quad (12)$$

where \vec{J}_{ℓ} are nuclear transition current matrix elements, and ℓ is a summation index over all possible transitions, with properties characterized by K_{ℓ} .¹⁵ This equation can be iteratively solved starting from an initial synchrotron radiation pulse $E(t) \sim \delta(t)$ which is instantaneous on the time scale of the nuclear dynamics.

A possibility for coherent control arises, if the iron nuclei are embedded in a suitable host material, such as FeBO_3 . Inside this crystal, the nuclei experience a strong magnetic field of order 30 T, leading to a pronounced Zeeman shift of the magnetic sublevels. Interestingly, the direction of this field can be controlled by a weak external magnetic field (tens of Gauss)

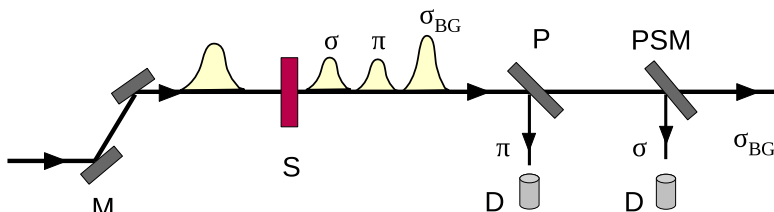


Fig. 10. Schematic setup for keV single photon entanglement generation. σ , π and σ_{BG} indicate the two signal components with σ and π polarization, and the background pulse, respectively. S is the target, and M is a monochromatizer. P and PSM are x-ray optics devices to separate the two signal pulses and to extract the signal from the background.

very rapidly. This feature can be facilitated to control the coherent decay of the nuclei.^{16,17} If directly after the excitation of the nuclei via the synchrotron radiation pulse the magnetic field is rotated, the excited upper sublevels are projected onto a new set of states determined by the new quantization axis after the rotation, see Fig. 9. If this switching occurs with a suitable rotation angle of the magnetic field, and at a suitable time, then the transition amplitudes for the coherent decay can destructively interfere, thus suppressing coherent decay. This mechanism is in close analogy to EIT, in which destructive interference of different transition channels prohibits an *excitation* of the atom. It was shown experimentally that this can lead to a storage of the upper state population over durations larger than the natural life time of the nuclei.¹⁶

Based on these ideas, it is possible to achieve single-photon mode entanglement at x-ray photon energies.¹⁷ Using an advanced switching scheme, the single excitation in the nuclei can be stored after the synchrotron pulse has passed by, and then be released into two subsequent separated pulses. The two pulses are distinct in the emission time and in the polarization of the emitted light. For this, after the excitation, the magnetic field is first rotated at a suitable time in direction parallel to the beam line. Until this point, all background light (the SR pulse and prompt electronic scattering) has left the target in a first pulse. At a suitable second switching time, the magnetic field is rotated back to release the first signal pulse with π -polarization. Then, another rotation in direction along the beam axis and rotation back at definite times leads to an emission of the second σ -polarized signal pulse, see Fig. 10. The obtained state is of the form

$$|\Psi\rangle = \alpha|0\rangle_A|1\rangle_B + \beta|1\rangle_A|0\rangle_B, \quad (13)$$

which is known as a single photon mode entangled state.¹⁸ Here, modes

A and B correspond to the different emitted pulses which have different polarizations. Using state-of-the-art x-ray optics, the two signal pulse components can then be extracted from the background, as indicated in Fig. 10 by the polarizing beam splitter (P) and time-variable mirror (PSM). The latter can either be realized using a Bragg-reflecting crystal mounted on a piezoelectric drive, or by facilitating mirror switching devices based on lattice deformations.

Nuclear forward scattering together with the magnetic field switching offers an interesting playground for coherent control of nuclear dynamics. Despite the weak interaction between light and nuclei, which on average leads to less than one excitation in the nuclei per incident pulse, a complete control of the coherent nuclear dynamics is enabled by the switching of the magnetic field. It can be expected that further applications in the coherent control of nuclei will arise from related techniques.

References

1. M. Fleischhauer, A. Imamoglu and J. P. Marangos, *Rev. Mod. Phys.* **77**, p. 633 (2005).
2. O. Kocharovskaya and P. Mandel, *Phys. Rev. A* **42**, p. 523 (1990).
3. C. H. Keitel, O. A. Kocharovskaya, L. M. Narducci, M. O. Scully, S.-Y. Zhu and H. M. Doss, *Phys. Rev. A* **48**, p. 3196 (1993).
4. G. Morigi, S. Franke-Arnold and G.-L. Oppo, *Phys. Rev. A* **66**, p. 053409 (2002).
5. E. A. Korsunsky and D. V. Kosachiov, *Phys. Rev. A* **60**, p. 4996 (1999).
6. M. Mahmoudi and J. Evers, *Phys. Rev. A* **74**, p. 063827 (2006).
7. R. Fleischhaker and J. Evers, *Phys. Rev. A* **80**, p. 063816 (2009).
8. G. Floquet, *Ann. École Norm. Sup.* **12**, p. 47 (1883).
9. R. Fleischhaker and J. Evers, *Phys. Rev. A* **78**, p. 051802 (2008).
10. A. Wicht, K. Danzmann, M. Fleischhauer, M. Scully, G. Müller and R. H. Rinkleff, *Opt. Commun.* **134**, p. 431 (1997).
11. G. S. Pati, M. Salit, K. Salit and M. S. Shahriar, *Phys. Rev. Lett.* **99**, p. 133601 (2007).
12. A. Dogariu, A. Kuzmich and L. J. Wang, *Phys. Rev. A* **63**, p. 053806 (2001).
13. J. Kästel, M. Fleischhauer, S. F. Yelin and R. L. Walsworth, *Phys. Rev. Lett.* **99**, p. 073602 (2007).
14. R. Röhlsberger, *Nuclear Condensed Matter Physics with Synchrotron Radiation: Basic Principles, Methodology and Applications (Springer Tracts in Modern Physics)* (Springer, 2004).
15. Y. V. Shvyd'ko, *Phys. Rev. B* **59**, 9132 (1999).
16. Y. V. Shvyd'ko, T. Hertrich, U. van Bürck, E. Gerdau, O. Leupold, J. Metge, H. D. Rüter, S. Schwendy, G. V. Smirnov, W. Potzel and P. Schindelmann, *Phys. Rev. Lett.* **77**, 3232 (1996).

17. A. Pálffy, C. H. Keitel and J. Evers, *Phys. Rev. Lett.* **103**, p. 017401 (2009).
18. S. J. van Enk, *Phys. Rev. A* **72**, p. 064306 (2005).